

On the line shape of the electrically detected ferromagnetic resonance

M. Harder¹, Z. X. Cao^{1,2}, Y. S. Gui¹, X. L. Fan^{1,3}, and C.-M. Hu^{1*}

¹*Department of Physics and Astronomy, University of Manitoba, Winnipeg, Canada R3T 2N2*

²*National Lab for Infrared Physics, Shanghai Institute of Technical Physics, Chinese Academy of Science, Shanghai 200083, People's Republic of China and*

³*The Key Lab for Magnetism and Magnetic Materials of Ministry of Education, Lanzhou University, Lanzhou 730000, People's Republic of China*

(Dated: September 30, 2018)

This work reviews and examines two particular issues related with the new technique of electrical detection of ferromagnetic resonance (FMR). This powerful technique has been broadly applied for studying magnetization and spin dynamics over the past few years. The first issue is the relation and distinction between different mechanisms that give rise to a photovoltage via FMR in composite magnetic structures, and the second is the proper analysis of the FMR line shape, which remains the "Achilles heel" in interpreting experimental results, especially for either studying the spin pumping effect or quantifying the spin Hall angles via the electrically detected FMR.

PACS numbers: 85.75.-d, 75.40.Gb, 76.50.+g, 42.65.-k

I. INTRODUCTION

Electrical detection of ferromagnetic resonance (FMR) in ferromagnets (FM) is a powerful new experimental tool which has transformed the research on spin and magnetization dynamics.¹⁻³³ Over the past few years, this technique has generated a great deal of interest in the communities of magnetism, spintronics, and microwave technologies. It has been broadly applied for studying diverse material structures, ranging from ferromagnetic thin films such as Py (permalloy, Ni₈₀Fe₂₀),^{4,6,12,13} CrO₂,¹⁴ Fe₃O₄,¹⁴ single crystal Fe,¹⁷ GaMnAs,¹⁸ and La_{1-x}Sr_xMnO₃,¹⁹ bilayer devices such as Py/Pt,^{7,8,20,21,25,26} Py/Au,^{20,21} Py/GaAs,²² and Y₃Fe₅O₁₂/Pt,^{23,24} to a variety of magnetic tunneling junctions (MTJ) based on magnetic multilayers.^{3,9-11} From a technical standpoint, its high sensitivity has made it possible to quantitatively determine spin boundary conditions²⁷ and to directly measure non-linear magnetization damping²⁸⁻³⁰, the quasiparticle mass for the domain wall³¹, the phase diagram of the the spin-transfer driven dynamics² and various kinds of parametric spin wave excitation^{2,32,33}. Its capability to probe the interplay of spins, charges, and photons has been utilized for studying spin rectification^{12,15}, spin pumping⁷, spin torque¹⁶, and spin Hall effects^{20,25,26}, which have led to the proposing and realization of novel dynamic spintronic devices such as the spin battery,^{7,34,35} spin diode,^{3,10,11} spin dynamo,^{12,15} and spin demodulator³⁶. Very recently, its ability to detect coherent processes³⁷⁻³⁹ has enabled electrical probing of the spin-resonance phase and the relative phase of electromagnetic waves³⁷, which pave new ways for microwave sensing⁴⁰, non-destructive imaging,³⁷ and dielectric spectroscopy³⁸. Such a coher-

ent capability is especially exciting as it resembles the latest achievement in semiconductor spintronics, where a new platform for coherent optical control of spin/charge currents has been developed by using nonresonant quantum interferences.⁴¹⁻⁴³

From the physical standpoint, many different effects may generate a time-independent dc voltage in magnetic materials via the FMR. Reported mechanisms involve spin rectification^{12,15}, spin pumping⁷, spin torque¹⁶, spin diode^{3,10,11}, spin Hall²⁵ and inverse spin Hall effects^{8,20,21,26}. Two major issues stand out here: (1) A unified picture clarifying the relations and distinctions between such diverse mechanisms has not been established, which leads to increasing controversy and confusion in interpreting and understanding experimental results. A stunning example of this issue is found in the very recent studies of the spin Hall effect via electrically detected FMR, where two similar experiments performed on similar devices were interpreted completely differently.^{20,25} (2) When more than one mechanism simultaneously plays a role in the FMR generated dc voltage, proper interpretation requires a quantitative analysis of the FMR line shape. In our opinion, this has remained the "Achilles heel" in recent studies of spin pumping and the spin Hall effect which utilize electrically detected FMR. The purpose of this article is to address these two critical issues with a brief review of the key physics of this subject, followed by systematically measured experimental data with detailed theoretical analysis.

This paper is split into three main sections. First we provide a brief review of different mechanisms which may generate the photovoltage via the FMR. Then we use the dynamic susceptibility obtained from a solution of the Landau-Lifshitz-Gilbert equation to derive analytical formulae for analyzing the line shape and the symmetry properties of the photovoltage generated through spin rectification. Finally we present experimental results measured from different samples, at different fre-

*Electronic address: hu@physics.umanitoba.ca; URL: <http://www.physics.umanitoba.ca/~hu>

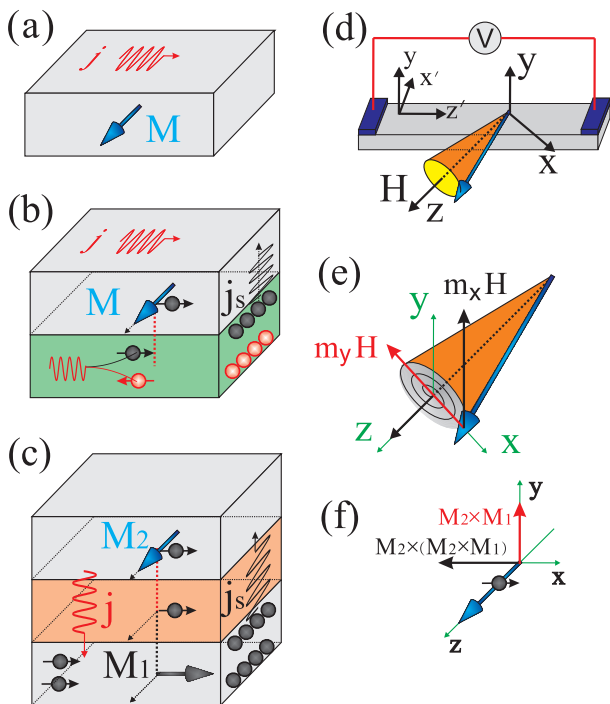


FIG. 1: (color online). Dynamic response of magnetic structures under microwave irradiation: (a) Single thin film layer where the spin rectification is due to the magnetic field torque as shown in (e). (b) Magnetic bilayer device which has two rf currents \mathbf{j} and \mathbf{j}_s with different spin polarizations. Therefore spin rectification is due to both magnetic field and spin torques. (c) Magnetic tunneling junction with both \mathbf{j} and \mathbf{j}_s . (d) Coordinate system for single ferromagnetic microstrips measured in this work under an in-plane applied static magnetic field \mathbf{H} . The z' -axis is fixed along the strip and the direction of current flow, while the z -axis is rotated to follow the direction of \mathbf{H} . (e) Components of magnetic field torque. (f) Spin torque in magnetic tunneling junction.

quencies, and in different experimental configurations, showing that the FMR line shape is determined by the relative phase of microwaves which is sample and frequency dependent.

II. A BRIEF REVIEW OF ELECTRICAL DETECTION OF FMR

Under microwave excitation at angular frequency ω , the rf electric (\mathbf{e}) and magnetic (\mathbf{h}) fields inside a ferromagnetic material can be described as $\mathbf{e} = \mathbf{e}_0 e^{-i\omega t}$ and $\mathbf{h} = \mathbf{h}_0 e^{-i(\omega t - \Phi)}$, respectively. Note that in general, due to the inevitable losses of microwaves propagating inside the ferromagnetic material, there is a phase difference Φ between the dynamic \mathbf{e} and \mathbf{h} fields. Such a relative phase is determined by the frequency-dependent wave impedance of the materials⁴⁴. As shown in Fig. 1, the rf \mathbf{e} field drives a rf current $\mathbf{j} = \sigma \mathbf{e}$, while the rf \mathbf{h} field exerts a field torque on the magnetization and

drives it to precess around its equilibrium direction [Fig. 1(e)]. Such a magnetization precession is described by the non-equilibrium magnetization $\mathbf{m} = \hat{\chi} \mathbf{h}$. Here σ and $\hat{\chi}$ are the high-frequency conductivity and Polder tensor, respectively. Note that due to the resonance nature of the precession, \mathbf{m} lags \mathbf{h} by a spin resonance phase Θ . However, despite the phase of Φ and Θ , the dynamic \mathbf{j} and \mathbf{m} keep the coherence of their respective driving fields, so that the product of any combination of their components may generate a time independent signal proportional to $\langle \text{Re}(\dot{\mathbf{j}}) \cdot \text{Re}(\dot{\mathbf{m}}) \rangle$, where $\langle \rangle$ denotes the time average. The amplitude of such a signal depends on the phase difference of \mathbf{j} and \mathbf{m} , which can be easily understood from the trigonometric relation: $\cos(\omega t) \cdot \cos(\omega t - \Phi) = [\cos(\Phi) + \cos(2\omega t - \Phi)]/2$. This is the spin rectification¹² as we highlight in Table I. For transport measurements on magnetic structures under microwave irradiation, various magnetoresistance effects such as anisotropic magnetoresistance (AMR), giant magnetoresistance (GMR) and tunneling magnetoresistance (TMR) make corrections to Ohm's law via their corresponding magnetoresistance terms^{15,45}. Such non-linear terms typically lead to the product of \mathbf{j} and \mathbf{m} . Spin rectifications induced by such magnetoresistance effects are listed in Table I by the terms labeled V_{MR} . The general feature of V_{MR} is that its amplitude depends on both the relative phase Φ and the spin resonance phase Θ , which leads to a characteristic phase signature of the FMR line shape^{37,38}.

Similar to the effect of the rf \mathbf{h} field torque, a spin torque induced by a spin polarized current may also drive magnetization precession. For example, in a bilayer [Fig. 1(b)] made of a ferromagnetic layer and a nonmagnetic layer with spin-orbit coupling²⁵, in addition to the rf current \mathbf{j} flowing in the ferromagnetic layer, the rf \mathbf{e} field also induces a rf charge current flowing in the nonmagnetic layer. Via the spin Hall effect in such a nonmagnetic layer with spin-orbit coupling, the rf charge current can be converted into a spin current \mathbf{j}_s , which may flow into the ferromagnetic layer and then drive the magnetization precession via the spin torque. Such a spin torque induced non-equilibrium magnetization can be described by $\mathbf{m} = \hat{\chi}_j \mathbf{j}_s$, where the spin-torque susceptibility tensor $\hat{\chi}_j$ introduces a spin resonance phase ϑ that is different from Θ in $\hat{\chi}$. Following a similar consideration for the magnetoresistance induced spin rectification, a photovoltage depending on the spin Hall effect may be generated in the ferromagnetic layer. This is the physical origin of the spin Hall induced spin rectification effect,²⁵ which is listed in Table I by the term labeled V_{SH} . In MTJ [Fig. 1(c)], the spin polarized current \mathbf{j}_s can be directly generated in the ferromagnetic layer where the magnetization is pinned along a different direction than that of the free layer. It tunnels into the free layer and drives the magnetization precession via the spin torque [Fig. 1(f)]. The induced spin rectification signal has been measured in spin diodes^{3,10,11}, which is listed in Table I by the term labeled V_{SD} .

Over the past few years, systematic studies on spin rectifications induced by the field (V_{MR}) and spin torque (V_{SH} , V_{SD}) have been performed, respectively, at the University of Manitoba^{12,15,17,18,27-29,37,38,40} and Cornell University^{2,9,11,16,25,48}. It has been found that due to the coherent nature of spin rectification, V_{MR} , V_{SH} and V_{SD} all depend on the phase difference between \mathbf{j} and \mathbf{m} . However, only the field torque spin rectification (V_{MR}) can be controlled by the relative phase Φ of the microwaves.³⁷

In addition to such coherent spin rectification effects, it is known that at the interface between a ferromagnetic and a nonmagnetic layer, microwave excitation may generate a spin polarized current flowing across the interface via the spin pumping effect³⁴. This effect has been observed in a few striking experiments by measuring either transmission electron spin resonance⁴⁶ or enhanced magnetization damping⁴⁷. It involves FMR, exchange coupling and non-equilibrium spin diffusion. In our opinion the physical picture of spin pumping was

best explained in the classical paper of Silsbee *et.al.* [Ref. 46], which highlighted the key mechanism of dynamic exchange coupling between the precessing magnetization and the spin polarized current. Such a dynamic coupling significantly "amplifies" the effect of the rf \mathbf{h} field in generating non-equilibrium spins. It was later proposed that the spin current generated via spin pumping may also induce a photovoltage, either across the interface in a spin battery^{7,34,35}, or within the nonmagnetic layer via the inverse spin Hall effect^{8,20,21,26}. Recent experiments performed on magnetic bilayers²⁵ have found that spin-pumping induced dc voltage (the term V_{SP} in Table I) should be about two orders of magnitude smaller than spin Hall induced spin rectification (the term labeled V_{SH}). In contrast to phase sensitive coherent spin rectification effects, the proposed spin-pumping photovoltage is based on incoherent spin diffusion and FMR absorption. Hence, the anticipated FMR line shape is symmetric and phase-independent.

TABLE I: Relation and distinctions between different mechanisms for microwave photovoltages induced by FMR. (For simplicity we consider only one matrix element of $\hat{\chi}$ and $\hat{\chi}_j$ which is responsible for the spin rectification. \tilde{j} and \tilde{m} denote a corresponding component of the time-dependent current and magnetization, respectively.)

| ac driving | $\tilde{e} = e_0 e^{-i\omega t}$ | $\tilde{j} = j_0 e^{-i\omega t}$ | $\tilde{h} = h_0 e^{-i(\omega t - \Phi)}$ | $\tilde{j}_s = j_s e^{-i\omega t}$ | | |
|------------|----------------------------------|----------------------------------|--|------------------------------------|--|------------------------|
| Effect | Ohm's law | spin Hall | field torque | spin torque | spin rectification | spin pumping |
| dc voltage | | | | | $V \sim \langle \text{Re}(\tilde{j}) \cdot \text{Re}(\tilde{m}) \rangle$ | $V \sim \tilde{m} ^2$ |
| Thin film | $\tilde{j} = \sigma \tilde{e}$ | | $\tilde{m} = \chi e^{i\Theta} \tilde{h}$ | | $V = V_{MR} \cdot (e_0 h_0)$ | |
| Bilayer | $\tilde{j} = \sigma \tilde{e}$ | \tilde{j}_s | $\tilde{m} = \chi e^{i\Theta} \tilde{h} + \chi_j e^{i\vartheta} \tilde{j}_s$ | | $V = V_{MR} \cdot (e_0 h_0) + V_{SH} \cdot (j_0 j_s) + V_{SP} \cdot m ^2$ | |
| MTJ | \tilde{j}, \tilde{j}_s | | $\tilde{m} = \chi e^{i\Theta} \tilde{h} + \chi_j e^{i\vartheta} \tilde{j}_s$ | | $V = V_{MR} \cdot (e_0 h_0) + V_{SD} \cdot (j_0 j_s)$ | |

V_{MR} : Spin Rectification caused by *MagnetoResistances*;^{12,13}

V_{SH} : Spin Rectification caused by *Spin Hall* effect;²⁵

V_{SD} : Spin Rectification caused by *Spin Diode* effect;^{3,10,11}

V_{SP} : Photovoltage caused by *Spin Pumping*.^{7,8,20,21,26}

From the above discussion, it is clear that the line shape analysis plays the essential role in distinguishing the microwave photovoltage generated by different mechanisms. This issue has been partially addressed by a number of theoretical^{48,49} and experimental works^{3,10,11}

studying nanostructured MTJs where the photovoltage is dominated by the spin torque induced spin rectification. Enlightened by these works and also based on our own previous studies^{15,37}, we discuss in the following the critical issue of FMR line shape analysis in microstruc-

tured devices, where the field and spin torque induced spin rectification may have comparable strength. Our theoretical consideration and experimental data demonstrate the pivotal role of the relative phase Φ , which was often under-estimated in previous studies. Via systematic studies with different device structures, measurement configurations and frequency ranges, we find that Φ has to be calibrated at different microwave frequencies for each device independently. Hence, our results are in strong contradiction with the recent experiment performed on microstructured magnetic bilayers for quantifying the spin Hall angles, where Φ was declared to be zero for all devices at different microwave frequencies^{20,21}.

III. FMR LINE SHAPE

A. The Characteristic Signature

From Table I, the role of the phase in the FMR line shape symmetry can be understood by considering the spin rectified voltage $V \propto \langle Re(\tilde{j}) \cdot Re(\tilde{m}) \rangle$. For spin rectification induced by the field torque, depending on the experimental configuration, at least one matrix component χ of the Polder tensor $\hat{\chi}$ will drive the FMR; whether an on or off-diagonal component is responsible for the magnetization precession depends on the measurement configuration. Since $\mathbf{m} = \hat{\chi}\mathbf{h}$, $Re(\tilde{m}) \propto Re(\chi) \cos(\omega t - \Phi) + Im(\chi) \sin(\omega t - \Phi)$. Therefore after time averaging a time independent dc voltage is found $V(\Phi) \propto [Re(\chi) \cos(\Phi) - Im(\chi) \sin(\Phi)]$. It is well known that for diagonal matrix elements, $Re(\chi)$ has a dispersive line shape while $Im(\chi)$ has a symmetric line shape. However since the on and off-diagonal susceptibilities differ by a phase of $\pi/2$, if the FMR is driven by an off-diagonal susceptibility, the roles are reversed and $Re(\chi)$ has a symmetric line shape while $Im(\chi)$ has a dispersive line shape.

Based on the simple argument leading to the above $V(\Phi)$ expression, one can see that the line shape symmetry has a characteristic dependence on the relative phase Φ between electric and magnetic fields. Thus when measuring FMR based on the field torque induced spin rectification effect, it is important to consider the relative phase, whereas for a spin pumping measurement which measures $|\mathbf{m}|^2$, or for a spin torque induced spin rectification which involves $|\mathbf{j}|^2$, the relative phase does not influence the experiment. In the next two sections, a detailed analysis is given by solving the Landau-Lifshitz-Gilbert equation, which leads to analytical formulae describing the symmetric and dispersive line shapes for different measurement configurations.

B. The Dynamic Susceptibility

The Landau-Lifshitz-Gilbert equation provides a phenomenological description of ferromagnetic dynamics based on a torque provided by the internal magnetic field \mathbf{H}_i which acts on the magnetization \mathbf{M} , causing it to precess⁵⁰

$$\frac{d\mathbf{M}}{dt} = -\gamma(\mathbf{M} \times \mathbf{H}_i) + \frac{\alpha}{M} \left(\mathbf{M} \times \frac{d\mathbf{M}}{dt} \right). \quad (1)$$

Here γ is the effective electron gyromagnetic ratio and α is the Gilbert damping parameter which can be used to determine the FMR line width ΔH , according to $\Delta H \sim \alpha\omega/\gamma$. For the case of microwave induced ferromagnetic resonance Eq. (1) can be solved by splitting the internal field into dc and rf components and taking the applied dc field \mathbf{H} , along the z -axis. We can relate the internal field $\mathbf{H}_i = \mathbf{H}_{0i} + \mathbf{h}_i e^{-i\omega t}$, to the applied field through the demagnetization factors N_k , $H_{0iz} = H - N_z M_0$, $h_{ik} = h_k e^{i\Phi_k} - N_k m_k$, where Φ_k is the relative phase shift between the electric and magnetic fields in the k^{th} direction and \mathbf{M}_0 is the dc magnetization also along the z -axis. With the magnetization separated into dc and rf contributions $\mathbf{M} = \mathbf{M}_0 + \mathbf{m} e^{-i\omega t}$, the solution of Eq. (1) yields the dynamic susceptibility tensor $\hat{\chi}$ which relates the magnetization \mathbf{m} to the externally applied rf field \mathbf{h}

$$\begin{aligned} \mathbf{m} &= \hat{\chi}\mathbf{h} = \begin{pmatrix} \chi_{xx} & i\chi_{xy} & 0 \\ -i\chi_{xy} & \chi_{yy} & 0 \\ 0 & 0 & 0 \end{pmatrix} \mathbf{h} \\ &= \begin{pmatrix} |\chi_{xx}| & |\chi_{xy}| e^{i\frac{\pi}{2}} & 0 \\ |\chi_{xy}| e^{-i\frac{\pi}{2}} & |\chi_{yy}| & 0 \\ 0 & 0 & 0 \end{pmatrix} \mathbf{h} e^{i\Theta}, \end{aligned} \quad (2)$$

where $\Theta = \arctan[\Delta H/(H - H_r)]$ is the spin resonance phase³⁷ which describes the phase shift between the response and the driving force in terms of the line width ΔH and the resonance field H_r which are constant for a fixed frequency. Θ will change from 180° (driving force out of phase) to 0° (driving force in phase) around the resonance position, in a range on the order of ΔH , passing through 90° at resonance. This represents the universal feature of a resonance; the phase of the dynamic response always lags behind the driving force.⁵¹

To emphasize the resonant feature of the susceptibility tensor elements we define the symmetric Lorentz line shape L , and the dispersive line shape D as

$$\begin{aligned} L &= \frac{\Delta H^2}{(H - H_r)^2 + \Delta H^2}, \\ D &= \frac{\Delta H(H - H_r)}{(H - H_r)^2 + \Delta H^2}. \end{aligned} \quad (3)$$

Clearly the spin resonance phase can also be written in terms of L and D as $\Theta = \arctan[\Delta H/(H - H_r)] =$

$\arctan(L/D)$ so that $L \propto \sin(\Theta)$ and $D \propto \cos(\Theta)$. Therefore L and D carry the resonant information of the susceptibility tensor.

Using L and D allows the elements of $\hat{\chi}$ to be written as $(\chi_{xx}, \chi_{xy}, \chi_{yy}) = (D + iL)(A_{xx}, A_{xy}, A_{yy})$. A_{xx}, A_{xy} and A_{yy} are real amplitudes which are related to the sample properties

$$\begin{aligned} A_{xx} &= \frac{\gamma M_0(M_0 N_y + (H - N_z M_0))}{\alpha \omega(2(H - N_z M_0) + M_0(N_z + N_y))}, \\ A_{xy} &= -\frac{M_0}{\alpha(2(H - N_z M_0) + M_0(N_z + N_y))}, \\ A_{yy} &= \frac{\gamma M_0(M_0 N_x + (H - N_z M_0))}{\alpha \omega(2(H - N_z M_0) + M_0(N_z + N_y))}. \end{aligned} \quad (4)$$

Since these amplitudes are real all components of $\hat{\chi}$ include both a dispersive and a Lorentz line shape determined solely from the $D + iL$ term. However, in a transmission experiment performed using a resonance cavity $|m|^2 \propto L^2 + D^2 = L$ is measured. This product removes the phase dependence carried by L and D and leaves only the Lorentz line shape. For the same reason, the microwave photovoltage induced by spin pumping (the V_{SP} term in Table I) has a symmetric line shape.

The susceptibility for the two cases of in-plane and perpendicularly applied dc magnetic fields can easily be found from Eq. (4) by using the appropriate demagnetization factors. When the lateral dimensions are much larger than the thickness, $N_x = N_z = 0$ and $N_y = 1$ for an in-plane field and $N_x = N_y = 0$ and $N_z = 1$ for a field applied at a small angle from the perpendicular. In this paper, we focus on the in-plane case. The line shape analysis for the perpendicular case can be found in Ref. 37. In both cases the form of the susceptibility, $\chi \propto D + iL$, describes the ferromagnetic resonance line shape where each element of $\hat{\chi}$ is the sum of an antisymmetric and symmetric Lorentz line shape. As we describe in the next section, via the V_{MR} term of the spin rectification effect, the symmetry properties of the dynamic susceptibility influence the symmetry of the electrically detected FMR which can be controlled by tuning the relative electromagnetic phase Φ .

C. Spin Rectification Induced by the Field Torque

The field-torque spin rectification effect results in the production of a dc voltage from the non-linear coupling of rf electric and magnetic fields. For example, it may follow from the generalized Ohm's law^{45,52}

$$\mathbf{J} = \sigma \mathbf{E}_0 - \frac{\sigma \Delta \rho}{M^2} (\mathbf{J} \cdot \mathbf{M}) \mathbf{M} + \sigma R_H \mathbf{J} \times \mathbf{M}, \quad (5)$$

where σ is the conductivity, $\Delta \rho$ is the resistivity change due to AMR and R_H is the extraordinary Hall coefficient.

As shown in Fig. 2, we use two coordinate systems to describe a long narrow strip under the rotating in-plane magnetic field \mathbf{H} . The sample coordinate system

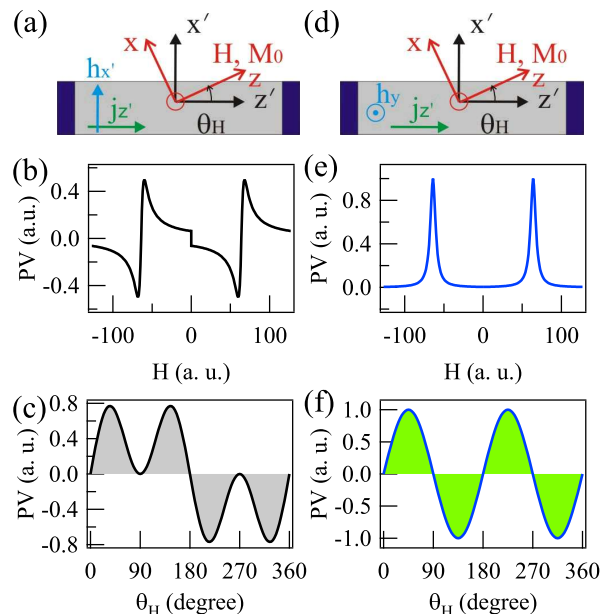


FIG. 2: (color online). Left panel (a) Coordinate system for an in-plane dc H field applied along the z -axis at an angle θ_H with respect to the z' -axis, with a rf h -field along the x' -axis. (b) The calculated photovoltage (PV) spectrum at $\theta_H = 45^\circ$ and (c) the calculated amplitude of the PV spectrum at FMR as a function of θ_H according to Eq. (9). Right Panel (d)-(f) are the same as (a)-(c), respectively, but with a rf h -field along the y -axis, and calculations are according to Eq. (10). In both cases, Φ is assumed to be zero.

$(\hat{x}', \hat{y}, \hat{z}')$ is fixed with the sample length along the z' direction and the sample width in the x' direction. The measurement coordinate system $(\hat{x}, \hat{y}, \hat{z})$ rotates with the \mathbf{H} direction which is along the \hat{z} axis. We define θ_H as the angle between the direction of the strip and the in-plane applied static magnetic field (*i.e.*, between the z' and z directions). In both coordinate systems, the \hat{y} axis is along the normal of the sample plane. In the case of a sample length much larger than the width, the rf current, $\tilde{j} = j_{z'} e^{-i\omega t}$ flows along the strip direction z' . In this geometry the field due to the Hall effect will only be in the transverse direction and will not generate a voltage along the strip. Taking the time average of the electric field integrated along the z' direction, the photovoltage is found as^{12,15}

$$V = \frac{\Delta R}{M_0} \langle \text{Re}(\tilde{j}) \cdot \text{Re}(\tilde{m}_x) \rangle \sin(2\theta_H), \quad (6)$$

where ΔR is the resistance change due to the AMR effect and the $\sin(2\theta_H)$ term is a result of the AMR effect which couples \mathbf{J} and \mathbf{M} .

The susceptibility tensor given by Eqs. (2) and (4) can be used to write \tilde{m}_x in terms of the rf \mathbf{h} field. Since \mathbf{M}_0 and \mathbf{H} are both along the z -axis, only the components of \mathbf{h} perpendicular to \mathbf{z} will contribute to \mathbf{m} . However, since the rf current flows in the z' direction, to calculate the rectified voltage, \tilde{m}_x must be transformed

into the (x', y, z') coordinate system by using the rotation $(\hat{\mathbf{x}}, \hat{\mathbf{y}}, \hat{\mathbf{z}}) = (\cos(\theta_H)\hat{\mathbf{x}}' - \sin(\theta_H)\hat{\mathbf{z}}', \hat{\mathbf{y}}, \sin(\theta_H)\hat{\mathbf{x}}' + \cos(\theta_H)\hat{\mathbf{z}}')$, which introduces an additional θ_H dependence into the photovoltage. We find that the photovoltage can be written in terms of the symmetric and antisymmetric Lorentz line shapes, L and D , as

$$V = \frac{\Delta R}{2M_0} j_{z'} (A_L L + A_D D), \quad (7)$$

where

$$\begin{aligned} A_L &= \sin(2\theta_H) [-A_{xx} h_{x'} \cos(\theta_H) \sin(\Phi_{x'}) \\ &\quad - A_{xy} h_y \cos(\Phi_y) + A_{xx} h_{z'} \sin(\theta_H) \sin(\Phi_{z'})], \\ A_D &= \sin(2\theta_H) [A_{xx} h_{x'} \cos(\theta_H) \cos(\Phi_{x'}) \\ &\quad - A_{xy} h_y \sin(\Phi_y) - A_{xx} h_{z'} \sin(\theta_H) \cos(\Phi_{z'})], \end{aligned} \quad (8)$$

and $\Phi_{x'}$, Φ_y and $\Phi_{z'}$ are the relative phases between electric and magnetic fields in the x' , y and z' directions, respectively.

The amplitudes of the Lorentz and dispersive line shape contributions show a complex dependence on the relative phases for the x' , y and z' directions and in general both line shapes will be present. However, depending on the experimental conditions, this dependence may be simplified. For instance when $h_{x'}$ is the dominate driving field as shown in Fig. 2(a), we may take $h_y = h_{z'} \approx 0$ and $\Phi_{x'} = \Phi$, which results in

$$V = -\frac{\Delta R}{2M_0} j_{z'} A_{xx} h_{x'} \cos(\theta_H) \sin(2\theta_H) [L \sin(\Phi) - D \cos(\Phi)]. \quad (9)$$

From Eq. (9) we see that the photovoltage line shape changes from purely symmetric to purely antisymmetric in 90° intervals of Φ , being purely antisymmetric when $\Phi = n \times 180^\circ$ and purely symmetric when $\Phi = (2n+1) \times 90^\circ$, $n = 0, \pm 1, \pm 2, \dots$

As shown in Fig. 2(b) and (c), the photovoltage in Eq. (9) also shows symmetries depending on the static field direction θ_H . Since $\mathbf{H} \rightarrow -\mathbf{H}$ corresponds to $\theta_H \rightarrow \theta_H + 180^\circ$, $V(H) = -V(-H)$. Furthermore at $\theta_H = n \times 90^\circ$, $n = 0, \pm 1, \pm 2, \dots$ the voltage will be zero.

Similarly when h_y dominates as shown in Fig. 2(c), we take $h_{x'} = h_{z'} \approx 0$ and $\Phi_y = \Phi$ which results in a voltage

$$V = -\frac{\Delta R}{2M_0} j_{z'} A_{xy} h_y \sin(2\theta_H) [L \cos(\Phi) + D \sin(\Phi)]. \quad (10)$$

The symmetry properties are now such that the line shape is purely symmetric when $\Phi = n \times 180^\circ$ and purely antisymmetric when $\Phi = (2n+1) \times 90^\circ$, $n = 0, \pm 1, \pm 2, \dots$. Also the photovoltage determined by Eq. (10) is now symmetric with respect to H under $\theta_H \rightarrow \theta_H + 180^\circ$ so that $V(H) = V(-H)$ as shown in Fig. 2(e). Therefore, experimentally the different symmetry

of the FMR at H and $-H$ can be used as an indication of which component of the \mathbf{h} field is dominant.

Both Eq. (9) and Eq. (10) demonstrate that a change in the relative electromagnetic phase is expected to result in a change in the line shape of the electrically detected FMR. It is worth noting that when the relative phase $\Phi = 0$, the line shape is purely antisymmetric for FMR driven by $h_{x'}$ and purely symmetric for FMR driven by h_y as illustrated in Fig. 2(b) and 2(e), respectively. In the general case when \tilde{m}_x is driven by multiple \mathbf{h} components, Eq. (7) must be used in combination with angular (θ_H) dependent measurements in order to distinguish different contributions.

D. The Physics of Φ

It is clear therefore that for field torque induced spin rectification, the relative phase Φ between the microwave electric and magnetic fields plays the pivotal role in the FMR line shape. Note that Φ is a material and frequency dependent property which is related to the losses in the system.^{44,54,55} When a plane electromagnetic wave propagates through free space the electric and magnetic fields are in phase and orthogonal to each other.⁵³ However when the same electromagnetic wave travels through a dispersive medium where the wave vector is complex, the imaginary contribution can create a phase shift between electric and magnetic fields. The most well known example is that of a plane electromagnetic wave moving in a conductor⁴⁴ where Faraday's law gives a simple relation between electric and magnetic fields, $\omega\mu\mathbf{h} = \mathbf{k} \times \mathbf{e}$. Therefore the complex part of the wave vector \mathbf{k} will induce a phase shift between electric and magnetic fields. Although the field will exponentially decay inside a conductor, it will still penetrate a distance on the order of the skin depth, and in a perfect conductor the conductivity, which produces an imaginary dielectric constant, will result in a phase shift of 45° between the electric and magnetic fields.⁴⁴

In a complex system such as an experimental set up involving waveguides, coaxial cables, bonding wires and a sample holder, which are required for electrical FMR detection, the relative phase cannot be simply calculated. Nevertheless losses in the system which can be characterized in a variety of ways, such as through the wave impedance,^{54,55} will lead to a phase shift between electric and magnetic fields which will influence the FMR line shape.

Although the physics of Φ is in principle contained in Maxwell's equations, due to the lack of technical tools for simultaneously and coherently probing both \mathbf{e} and \mathbf{h} fields, the effect of the relative phase had often been ignored until the recent development of spintronic Michelson interferometry³⁷. In the following we provide systematically measured data showing the influence of the relative phase Φ on the line shape of FMR which is driven by different \mathbf{h} field components.

IV. EXPERIMENTAL LINE SHAPE MEASUREMENTS

A. h_y Dominant FMR

In order to use the h_y field to drive FMR a first generation spin dynamo was used where a Cu/Cr coplanar waveguide (CPW) was fabricated beside a Py microstrip with dimension $300 \mu\text{m} \times 20 \mu\text{m} \times 50 \text{nm}$ on a SiO_2/Si substrate as shown in Fig. 3(a). A microwave current is directly injected into the CPW and flows in the z' direction inducing a current in the Py strip also along the z' -axis. In this geometry the dominant rf \mathbf{h} field in the Py will be the Oersted field in the y direction produced according to Ampère's Law. This field will induce FMR precession with the same cone angle independent of the static \mathbf{H} orientation.

The AMR resistance depends on the orientation of the magnetization relative to the current and follows the relation $R(H) = R(0) - \Delta R \sin^2(\theta_M)$, where θ_M (not shown) is the angle between the magnetization and the current direction. For Py the AMR effect, which is responsible for the spin rectification, is observed to produce a resistance change of $\Delta R/R(0) \sim 0.4\%$. When \mathbf{H} is applied along the x' -axis, *i.e.*, the in-plane hard axis, the magnetization \mathbf{M} tends to align toward the static field \mathbf{H} and the angle θ_M is determined by $\sin(\theta_M) = H/H_A$ for $H < H_A$, where $H_A = N_{x'}M_0$ is the in-plane shape anisotropy field. The measured data (symbols) shown in Fig. 3(c) is fit (solid curve) according to $R(H) = R(0) - \Delta R \sin^2(\theta_M)$ with $R(0) = 112.66 \Omega$, $\Delta R = 0.47 \Omega$, $\mu_0 H_A = 4.0 \text{ mT}$, and $N_{x'} = 0.004$.

Fig. 3(d) shows that the line shape at $\theta_H = 120^\circ$ and $\omega/2\pi = 5 \text{ GHz}$ is almost purely dispersive, indicating that at this frequency $\Phi \sim 90^\circ$ according to Eq. (10). The θ_H dependence of H_r is shown in Fig. 3(e) and can be well fit by the function $\omega = \gamma \sqrt{(|H_r| + H_A \cos(2\theta_H))(|H_r| + M_0 - H_A(1 + \sin^2(\theta_H)))}$ by taking the shape anisotropy field H_A along the x' -axis into account.⁵⁶ As expected the amplitude of these oscillations is $\mu_0 H_A = 4.0 \text{ mT}$. The frequency dependence of H_r at $\theta_H = 45^\circ$ is shown in Fig. 3(f) and is fit using $\omega = \gamma \sqrt{|H_r|(|H_r| + M_0)}$ with $\gamma/2\pi = 29.0 \mu_0 \text{ GHz/T}$ and $\mu_0 M = 1.0 \text{ T}$.

By systematically measuring the line shape as a function of the microwave frequency, we observe the interesting results of Fig. 4. The FMR line shape is observed to change from almost purely dispersive at $\omega/2\pi = 5 \text{ GHz}$ to almost purely symmetric at $\omega/2\pi = 5.56 \text{ GHz}$. As discussed before, the line shape may be affected by the \mathbf{h} orientation, *i.e.*, different \mathbf{h} vector components will affect the line shape differently. Hence, if changing the microwave frequency changes the dominant driving field, the line shape may change. To rule out such a possibility an angular dependent experiment was performed to measure the line shape at different θ_H for each frequency ω . The results are plotted on the right panel of Fig. 4

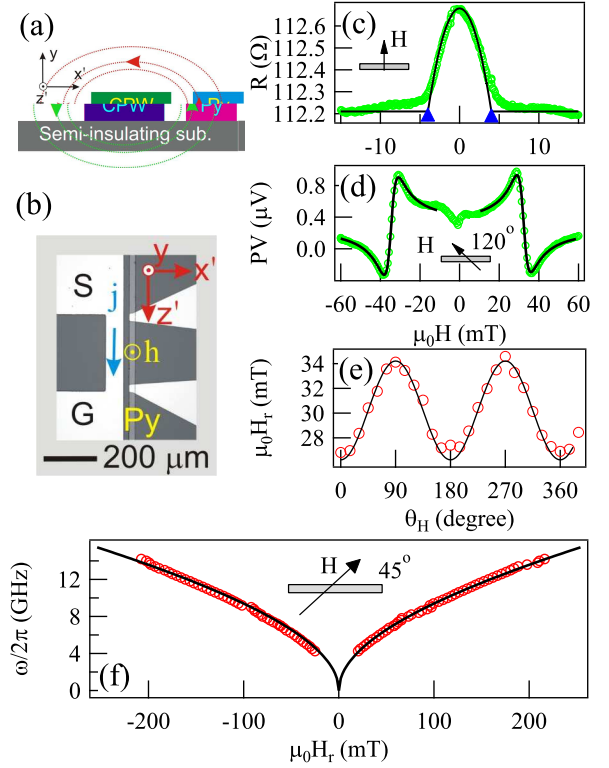


FIG. 3: (color online). (a) Schematic diagram of the first generation spin dynamo where the Py strip is located beside the CPW. The dominate magnetic field in the Py is the Oersted field in the y direction due to the current in the CPW. (b) Micrograph of the device. (c) Magnetoresistance at $\theta_H = 90^\circ$. AMR is seen to be $\sim 0.4\%$. Arrows denote the anisotropic field, $\mu_0 H_A = 4.0 \text{ mT}$. Open circles are experimental data and solid curve is the fitting result using $R(0) = 112.66 \Omega$, $\Delta R = 0.47 \Omega$, $H_A = 4.0 \text{ mT}$. (d) Electrically detected FMR at $\theta_H = 120^\circ$ and $\omega/2\pi = 5 \text{ GHz}$ showing an almost purely dispersive line shape ($\Phi \simeq 90^\circ$). Fit is according to Eq. (10) with $\mu_0 \Delta H = 3.6 \text{ mT}$, $\mu_0 H_r = 32.2 \text{ mT}$. (e) Oscillating H_r dependence on the static field direction θ_H with amplitude $2H_A$. (f) Dependence of FMR frequency on the resonant field H_r at $\theta_H = 45^\circ$. Open circles are experimental data and the solid line is the fit according to $\omega = \gamma \sqrt{|H_r|(|H_r| + M_0)}$.

which shows the sinusoidal curves for the Lorentz, A_L , and dispersive, A_D , amplitudes (dashed and solid curves respectively) as a function of the static field angle θ_H . Both the Lorentz and dispersive amplitudes are found to follow a $\sin(2\theta_H)$ dependence on the field angle in agreement with Eq. (10) indicating that the magnetization precession is indeed dominantly driven by the h_y field. Therefore the line shape change indicates that the relative phase Φ is frequency dependent. As shown in Fig. 5(a), at $\omega/2\pi = 5 \text{ GHz}$ the amplitude of A_D is approximately one order of magnitude larger than A_L , while at $\omega/2\pi = 5.56 \text{ GHz}$ A_D is one order of magnitude less than A_L . Such a large change in A_L/A_D shows that in a microwave frequency range as narrow as 0.6 GHz, the

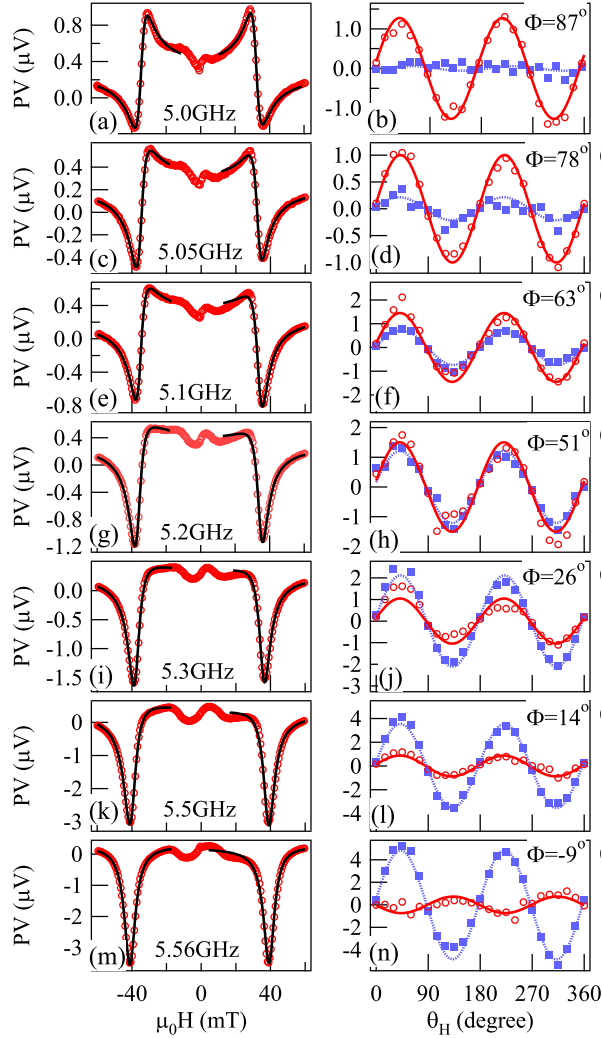


FIG. 4: (color online). Data shown for a first generation spin dynamo. FMR spectra at $\theta_H = 120^\circ$ for several frequencies from 5.0 to 5.56 GHz with corresponding Lorentz and dispersive amplitudes as a function of θ_H . Circles and squares indicate the Lorentz and dispersive amplitudes of Eq. (10) respectively and show a $\sin(2\theta_H)$ dependence as expected. Solid and dashed curves are $\sin(2\theta_H)$ functions.

relative phase Φ can change by 90° . Fig. 5(b) shows Φ determined by using Eq. (10), which smoothly changes with microwave frequency except for a feature near 5.18 GHz, which is possibly caused by a resonant waveguide mode at this frequency.

Such a large change of Φ within a very narrow range of microwave frequency indicates the complexity of wave physics. Note that microwaves at ~ 5 GHz have wavelengths on the order of a few centimeters which are much larger than the sub-millimeter sample dimensions. Consequently the microwave propagation depends strongly on the boundary conditions of Maxwell's equations which physically include the bonding wire, chip carrier, as well as the sample holder. This is similar to the microwave

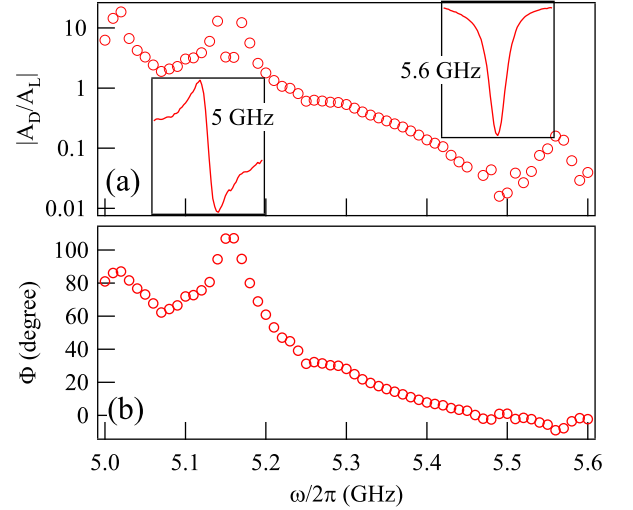


FIG. 5: (color online). (a) The A_D/A_L ratio as a function of $\omega/2\pi$ showing the line shape change from dispersive at 5 GHz (left inset) to Lorentz at 5.6 GHz (right inset) with a step size of 0.01 GHz. (b) Φ dependence on $\omega/2\pi$ over same frequency interval showing the same dependence as A_D/A_L .

propagation in a waveguide where the field distribution *i.e.* the waveguide modes, are known to depend strongly on boundary conditions and frequency.⁵⁷ Despite the complex wave properties, the key message of our results is clear and consistent with the consideration of the physics of the relative phase: it shows that in order to properly analyze the FMR line shape, Φ has to be determined for each frequency independently.

B. $h_{x'}$ Dominant FMR

In order to drive the FMR using the rf field in the x' direction, $h_{x'}$, a second generation spin dynamo was fabricated with the Py strip underneath the CPW as shown in Fig. 6. In this case the $300 \mu\text{m} \times 7 \mu\text{m} \times 100 \text{nm}$ Py strip is underneath the Cu/Cr coplanar waveguide which is fabricated on a SiO_2/Si substrate. Again a microwave current is directly injected into the CPW and induces a current in the z' direction in the Py strip. The dominant rf field in the Py is still the Oersted field, but due to the new geometry it is in the x' direction.

Due to the smaller width and larger thickness, the demagnetization factor, $N_{x'} = 0.008$ is twice that in the first generation sample. This corresponds to $\mu_0 H_A = 8.0 \text{ mT}$ as indicated by the broader AMR curve in Fig. 6(c). This value is further confirmed by the H_r vs θ_H plot shown in Fig. 6(e). Fig. 6(f) shows the frequency dependence of H_r for FMR (circles) and for the first perpendicular standing spin wave resonance (SWR) (triangles) measured at $\theta_H = 45^\circ$. The frequency dependence of H_r follows $\omega = \gamma \sqrt{(|H_r| + H_{ex})(|H_r| + M_0 + H_{ex})}$ where H_{ex} is the exchange field. In Fig. 6(f) the standing

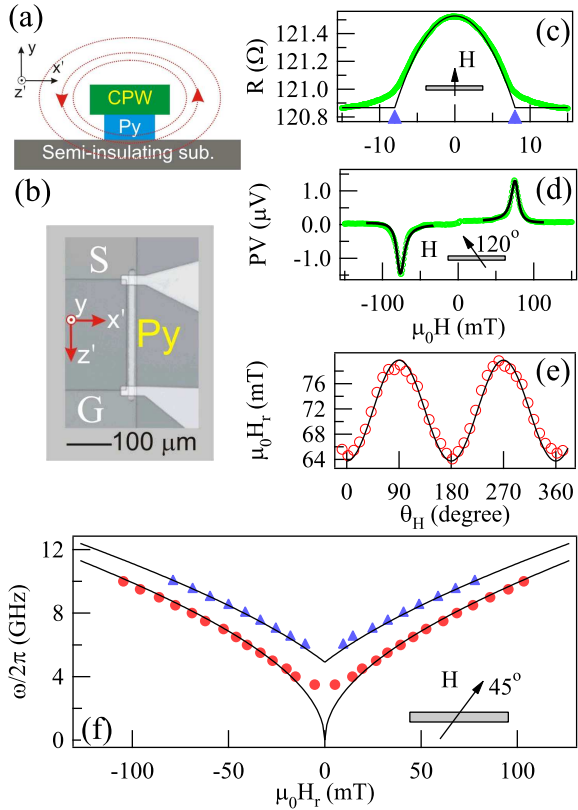


FIG. 6: (color online). (a) Schematic diagram of the second generation spin dynamo where the Py strip is located underneath the CPW. In this case the dominant magnetic field in the Py is the Oersted field in the x' direction due to the field in the CPW. (b) Micrograph of the Py CPW device. (c) Magneto-resistance at $\theta_H = 90^\circ$. AMR is seen to be $\sim 0.5\%$. Arrows denote the anisotropic field, $\mu_0 H_A = 8.0$ mT. Open circles are experimental data and solid curve is the fitting result using $R(0) = 121.53 \Omega$ and $\Delta R = 0.66 \Omega$. (d) Electrically detected FMR at $\theta_H = 120^\circ$ and $\omega/2\pi = 8$ GHz showing a nearly symmetric Lorentz line shape. Fit is according to Eq. (10) with $\mu_0 \Delta H = 6.0$ mT, $\mu_0 H_r = 76.5$ mT and $\Phi = -102^\circ$. (e) Oscillating H_r dependence on the static field direction θ_H with amplitude $2H_A$. (f) Dependence of FMR frequency on the resonant field H_r at $\theta_H = 45^\circ$. Solid circles show the FMR frequency dependence while the solid triangles are the standing SWR frequency dependence. The solid line is a fit to $\omega = \gamma \sqrt{|H_r|(|H_r| + M_0)}$.

SWR is fit using $\gamma/2\pi = 29.0 \mu_0 \text{GHz/T}$, $\mu_0 H_{ex} = 30$ mT and $\mu_0 M_0 = 1.0$ T.

Similar to the results presented in the previous section, the line shape of FMR measured on the second generation sample is also found to be frequency dependent (not shown). Hence, Φ is found to be non-zero in the general case. For example, at $\omega/2\pi = 8$ GHz, the line shape is found to be nearly symmetric, as shown in Fig. 6(d) for the FMR measured at $\theta_H = 120^\circ$, which indicates Φ is close to -90° at this frequency. Note that our result is in direct contrast with the recent study of Ref. 20 and 21, where experiments were measured in the same con-

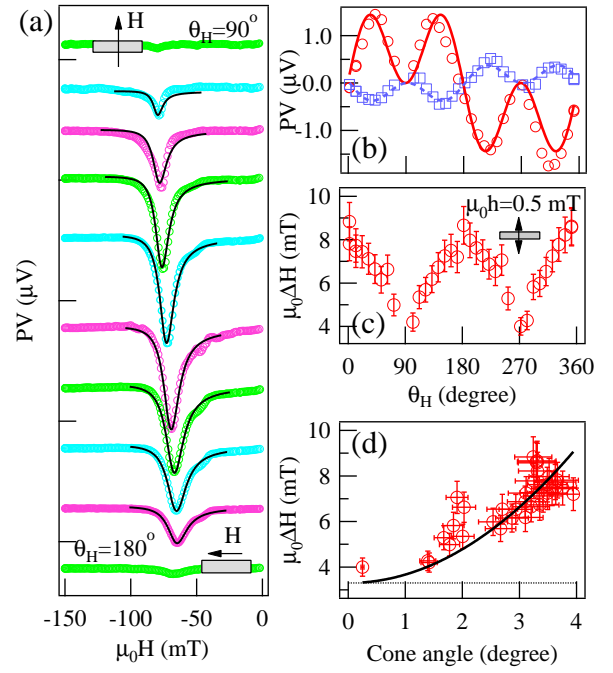


FIG. 7: (color online). Data shown for a second generation spin dynamo. (a) FMR line shape at fixed frequency, $\omega/2\pi = 8$ GHz for several θ_H from 90° to 180° in steps of 10° . Open circles are experimental data and solid lines are fits using Eq. (9) with $\Phi = -102^\circ$ fixed. (b) A_D and A_L shown in squares and circles respectively as a function of θ_H . Fitting curves are $\sin(2\theta_H) \cos(\theta_H)$ functions. (c) ΔH for several values of θ_H showing an oscillation with θ_H . (d) Non-linear dependence of line width ΔH on the cone angle. Dashed line is the expected linear Gilbert damping whereas the data follows the quadratic dependence shown by the solid line.

figuration and where it was suggested that $\Phi = 0^\circ$ for all samples at all frequencies.

While the line shape and hence the relative phase is found to be frequency dependent, Φ is expected to be independent of the static field direction θ_H . This is confirmed in Fig. 7(a) which shows the line shape measured at several values of θ_H in 10° increments. The data can be fit well using Eq. (9) with a constant $\Phi = -102^\circ$ for all θ_H . It confirms that the FMR is driven by a single \mathbf{h} component, in this case the $h_{x'}$ field, and that Φ does not depend on θ_H . In Fig. 7(b) the θ_H dependence of A_L and A_D (solid/circles and dashed/squares respectively) is shown. The circles and squares are experimental data while the solid and dashed lines are fitting results using a $\sin(2\theta_H) \cos(\theta_H)$ function according to Eq. (9). It provides further proof that the $h_{x'}$ field is responsible for driving the FMR in this sample.

While the results from both the 1st and 2nd generation spin dynamos show consistently that Φ is sample and frequency dependent, the 2nd generation spin dynamos exhibit special features in comparison with the 1st generation spin dynamos: the reduced separation between the Py strip and CPW enhances the $h_{x'}$ field so that the

line width ΔH is enhanced by non-linear magnetization damping^{28,29,58}, which depends on the cone angle θ of the precession via the relation $\theta \sim h_{x'} \cos(\theta_H) / \Delta H(\theta)$. As shown in Fig. 7(c), ΔH is found to oscillate between 4.0 and 9.0 mT as θ_H changes. At $\theta_H = 0^\circ$, $\theta \sim h_{x'} / \Delta H$ and the cone angle is at its largest (about 4°). As θ_H increases from 0° and moves toward 90° , θ decreases so that the non-linear damping contribution to ΔH decreases. Using the cone angle calculated from Fig. 7(c), we plot in Fig. 7(d) $\Delta H(\theta)$ as a function of the cone angle. It shows that ΔH has a quadratic dependence on the precession cone angle, which is in agreement with our previous study in the perpendicular \mathbf{H} -field configuration^{28,29}. We note that for cone angles above only a few degrees, the non-linear damping already dominates the contribution to ΔH . Again, this is in direct contrast with the result of Mosendz *et al.*,^{20,21}, where ΔH was found to be constant by varying θ_H , indicating no influence from non-linear damping, but the cone angle θ was estimated to be as high as 15° based on the line shape analysis assuming relative phase $\Phi = 0$.

C. Arbitrary \mathbf{h} Vector

Next we consider the most general case which is described by Eq. (7) where all components of \mathbf{h} may contribute to the FMR line shape. The sample used here is a single Py strip where a waveguide with a horn antennae provided both the electric and magnetic driving fields. The sample chip is mounted near the centre, at the end of a rectangular waveguide and the Py strip is directed along the short axis of the waveguide.

In a waveguide, the electromagnetic fields are well known and in general three components, $h_{x'}$, h_y and $h_{z'}$ exist.⁵⁷ Figure 8(a) shows both the FMR and perpendicular standing SWR at $\theta_H = 45^\circ$. Indeed both the amplitude and the line shape are different for the two FMR peaks located at H and $-H$, which indicates the existence of multiple \mathbf{h} field components and Eq. (7) and Eq. (8) are needed to separate them.

This separation is done using the Lorentz and dispersive amplitudes determined from a fit to the FMR which are plotted as a function of θ_H in Fig. 8(b) and (c) for $\omega/2\pi = 12$ and 11.2 GHz, respectively. A fit using Eq. (8) allows a separation of the contributions from each of the $h_{x'}$, h_y and $h_{z'}$ fields based on their different contributions to the θ_H dependence of the line shape.

The results of the fit have been tabulated in Table II where $\gamma/2\pi = 28.0 \mu\text{O GHz/T}$, $\mu_0 M_0 = 0.97 \text{ T}$ and $\mu_0 H_r = 152 \text{ mT}$ were used. The amplitudes of the different \mathbf{h} field components have been normalized with respect to the $h_{x'}$ component. At both 11.2 and 12 GHz the $h_{x'}$ field is much larger than h_y or $h_{z'}$, which is expected based on the wave propagation in a horn antennae.

In changing from 11.2 to 12 GHz the relative phase for each component is seen to change. Therefore even in the case of a complex line shape produced by multiple \mathbf{h} field

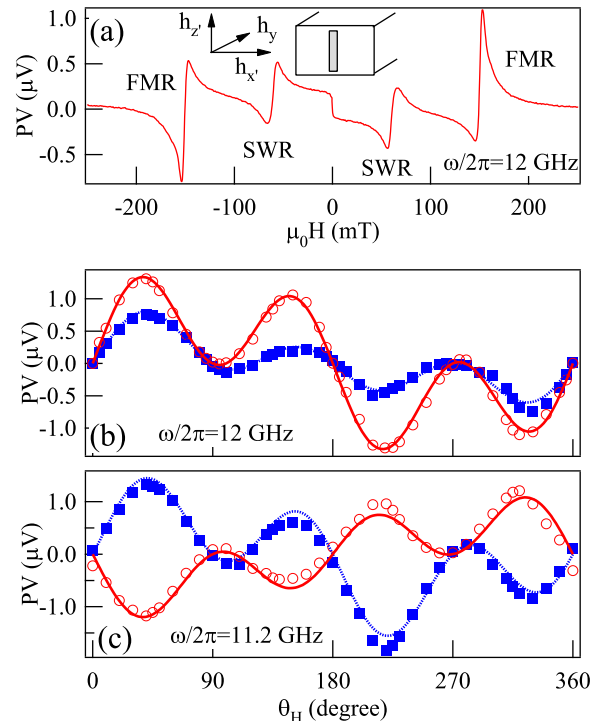


FIG. 8: (color online). Data shown for a single Py strip with precession driven by horn antennae field. The strip dimensions are $3 \text{ mm} \times 50 \mu\text{m} \times 45 \text{ nm}$. (a) Spectra showing distinct resonances due to FMR and SWR at $\omega/2\pi = 12 \text{ GHz}$. (b) Separated Lorentz and dispersive line shapes (circles and squares respectively) as a function of θ_H from a fit to Eq. (7) at $\omega/2\pi = 12 \text{ GHz}$ and (c) $\omega/2\pi = 11.2 \text{ GHz}$.

TABLE II: Angular separation of \mathbf{h} field components for 12 and 11.2 GHz.

| | 12 GHz | 11.2 GHz |
|-------------|-------------|-------------|
| $ h_{x'} $ | 1 | 1 |
| $ h_y $ | 0.02 | 0.14 |
| $ h_{z'} $ | 0.19 | 0.37 |
| $\Phi_{x'}$ | -23° | 50° |
| Φ_y | 40° | -30° |
| $\Phi_{z'}$ | -33° | 82° |

components, by separating the individual contributions of the rf magnetic field via angular dependence measurements, the relative phase Φ of each field component is found to be frequency dependent.

D. Additional Influences on Φ

In addition to the frequency and sample dependencies, the relative phase Φ may also depend on the lead configuration and wiring conditions of a particular device, as we have mentioned in Section A. Here, we address such additional influences by using the first generation spin

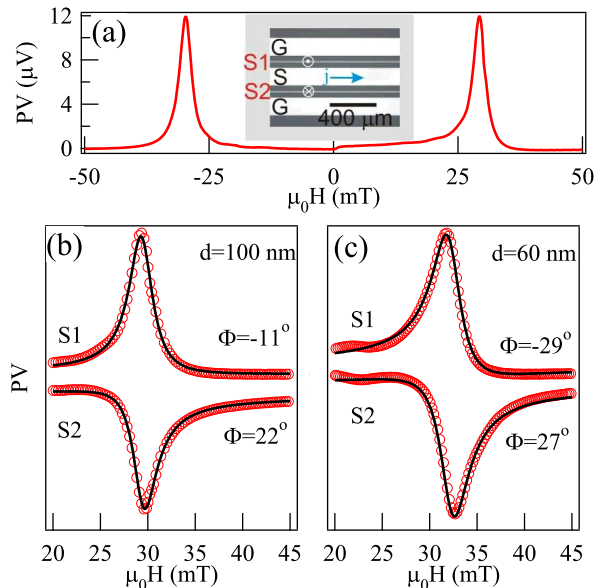


FIG. 9: (color online). (a) FMR observed in a first generation spin dynamo. Inset shows the device structure with two Py strips labeled S1 and S2. (b) FMR for Py thickness $d = 100$ nm for both S1 and S2. In S1 $\Phi = -11^\circ$, while in S2 the line shape is slightly more asymmetric and $\Phi = 22^\circ$. (c) For $d = 60$ nm the relative phase is $\Phi = -29^\circ$ for S1 and $\Phi = 27^\circ$ for S2.

dynamos¹² shown in the inset of Fig. 9(a). Two spin dynamos with the same lateral dimensions but different Py thickness d are studied. Each spin dynamo involves two identical Py strips denoted by S1 and S2, one in each center of the G-S strips of the CPW, which are placed symmetrically with respect to the S strip. The current and rf \mathbf{h} field are induced in the Py via a microwave current directly injected into the CPW. Similar to the sample discussed in Section A, h_y is the dominant field which drives the FMR.

As shown in Fig. 9(a), FMR measured at $\omega/2\pi = 5$ GHz on the sample S1 with $d = 100$ nm shows a nearly symmetric Lorentz line shape and a field symmetry of $V(H) = V(-H)$. From the FMR line shape fitting, $\Phi = -11^\circ$ is found. Interestingly, as shown in Fig. 9(b), the FMR of the sample S2 of the same spin dynamo measured under the same experimental conditions shows a different line shape, from which a different $\Phi = 22^\circ$ is found. We can further compare Φ measured on the other spin dynamo with a different Py thickness of $d = 60$ nm, also at $\omega/2\pi = 5$ GHz. Here for S1, $\Phi = -29^\circ$ while for S2, $\Phi = 27^\circ$. Again, the relative phase is found different for S1 and S2. These results demonstrate that due to additional influences such as a different lead configuration and wiring conditions, even for samples with the same lateral dimensions, Φ in each device is not necessarily the same. It demonstrates clearly that the relative phase Φ can not be simply determined by analyzing the

FMR line shape measured on a reference device.

E. Closing Remarks

The experimental data presented above show that regardless of the FMR driving field configuration, the relative phase between the rf electric and magnetic field is sample and frequency dependent and non-zero. This non-zero phase results in both symmetric and antisymmetric Lorentz line shapes in the FMR detected via field-torque induced spin rectification. The Φ dependence of the line shape symmetry changes based on which component of the rf \mathbf{h} field is responsible for driving the FMR precession. For instance a purely antisymmetric line shape could correspond to $\Phi = 0^\circ$ if the FMR is driven by h_x , or to $\Phi = 90^\circ$ if the FMR is driven by h_y , therefore the line shape itself cannot be used to determine Φ directly. To separate the \mathbf{h} field components an angular (θ_H) dependence measurement is necessary, which allows both \mathbf{h} as well as the phase to be determined. Using such a measurement Φ has been observed to change from 0° to 90° in a narrow frequency range (0.6 GHz) resulting in a change from an antisymmetric to symmetric line shape demonstrating the large effect the relative phase has on the FMR line shape. Furthermore Φ is not identical even in samples with the same geometrical size. Therefore in our opinion Φ cannot be simply determined from a reference sample but should be calibrated for each sample, at each frequency and for each measurement cycle.

V. CONCLUSION

Spin rectifications caused by the coupling between current and magnetization in a ferromagnetic microstrip provide a powerful tool for the study of spin dynamics. In order to distinguish different mechanisms which enable the electrical detection of FMR via microwave photovoltages, it is essential to properly analyze the FMR line shape. For spin rectification caused by a microwave field torque, due to the coherent nature of this coupling, the resulting dc voltage depends strongly on the relative phase between the rf electric and magnetic fields used to drive the current and magnetization, respectively. Therefore not only does electrical FMR detection provide a route to study the relative phase, but it also necessitates calibrating the relative phase prior to performing electrically detected FMR experiments. Based on a systematic study of the electrically detected FMR, the line shape is observed to depend strongly on the microwave frequency, driving field configuration, sample structure and even wiring conditions. It is in general a combination of Lorentz and dispersive contributions. These effects have been quantitatively explained by accounting for the relative phase shift between electric and magnetic fields. Analytical formulae have been established to analyze the FMR line shape. Our results imply that for

electrically detected FMR which involves both spin Hall and spin rectification effects, the pivotal relative phase must be calibrated independently in order to properly analyze the FMR line shape and quantify the spin Hall angle. This cannot be done by using a reference sample but could be achieved through such techniques as spintronic Michelson interferometry³⁷.

ACKNOWLEDGEMENTS

We would like to thank B. W. Southern, A. Hoffmann, and S. D. Bader for discussions. This work has been funded by NSERC, CFI, CMC and URGP grants (C.-M. H.). ZXC was supported by the National Natural Science Foundation of China Grant No. 10990100.

- ¹ M. Tsoi, A. G. M. Jansen, J. Bass, W.-C. Chiang, V. Tsoi, and P. Wyder, *Nature (London)* **406**, 46 (2000).
- ² S. I. Kiselev, J. C. Sankey, I. N. Krivorotov, N. C. Emley, R. J. Schoelkopf, R. A. Buhrman, and D. C. Ralph, *Nature (London)* **425**, 380 (2003).
- ³ A. A. Tulapurkar, Y. Suzuki, A. Fukushima, H. Kubota, H. Maehara, K. Tsunekawa, D. D. Djayaprawira, N. Watanabe and S. Yuasa, *Nature (London)* **438**, 339 (2005).
- ⁴ Y. S. Gui, S. Holland, N. Mecking, and C.-M. Hu, *Phys. Rev. Lett.* **95**, 056807 (2005).
- ⁵ A. Azevedo, L. H. Vilela Leo, R. L. Rodriguez-Suarez, A. B. Oliveira, and S. M. Rezende, *J. Appl. Phys.* **97**, 10C715 (2005).
- ⁶ M. V. Costache, S. M. Watts, M. Sladkov, C. H. van der Wal, and B. J. van Wees, *Appl. Phys. Lett.* **89**, 232115 (2006).
- ⁷ M. V. Costache, M. Sladkov, S. M. Watts, C. H. van der Wal, and B. J. van Wees, *Phys. Rev. Lett.* **97**, 216603 (2006).
- ⁸ E. Saitoh, M. Ueda, H. Miyajima, and G. Tatara, *Appl. Phys. Lett.* **88**, 182509 (2006).
- ⁹ J. C. Sankey, P. M. Braganca, A. G. F. Garcia, I. N. Krivorotov, R. A. Buhrman, and D. C. Ralph, *Phys. Rev. Lett.* **96**, 227601 (2006).
- ¹⁰ H. Kubota, A. Fukushima, K. Yakushiji, T. Nagahama, S. Yuasa, K. Ando, H. Maehara, Y. Nagamine, K. Tsunekawa, D. D. Djayaprawira, N. Watanabe, and Y. Suzuki, *Nature Physics* **4**, 37 (2007).
- ¹¹ J. C. Sankey, Y. T. Cui, J. Z. Sun, J. C. Slonczewski, Robert A. Buhrman, and D. C. Ralph, *Nature Physics* **4**, 67 (2007).
- ¹² Y. S. Gui, N. Mecking, X. Zhou, G. Williams and C. -M. Hu, *Phys. Rev. Lett.* **98**, 107602 (2007).
- ¹³ A. Yamaguchi, H. Miyajima, T. Ono, Y. Suzuki, S. Yuasa, A. Tulapurkar, and Y. Nakatani, *Appl. Phys. Lett.* **90**, 182507 (2007).
- ¹⁴ S. T. Goennenwein, S. W. Schink, A. Brandmaier, A. Boger, M. Opel, R. Gross, R. S. Keizer, T. M. Klapwijk, A. Gupta, H. Huebl, C. Bihler, and M. S. Brandt, *Appl. Phys. Lett.* **90**, 162507 (2007).
- ¹⁵ N. Mecking, Y. S. Gui, and C.-M. Hu, *Phys. Rev. B* **76**, 224430 (2007).
- ¹⁶ J. C. Sankey, Y. T. Cui, J. Z. Sun, J. C. Slonczewski, R. A. Buhrman and D. C. Ralph, *Nature Physics*, **4**, 67 (2008)
- ¹⁷ X. Hui, A. Wirthmann, Y. S. Gui, Y. Tian, X. F. Jin, Z. H. Chen, S. C. Shen, and C. -M. Hu, *Appl. Phys. Lett.* **93**, 232502 (2008).
- ¹⁸ A. Wirthmann, X. Hui, N. Mecking, Y. S. Gui, T. Chakraborty, C. -M. Hu, M. Reinwald, C. Schüller, and W. Wegscheider, *Appl. Phys. Lett.* **92**, 232106 (2008).
- ¹⁹ V. A. Atsarkin, V. V. Demidov, L. V. Levkin, and A. M. Petrzikh, *Phys. Rev. B* **82**, 144414 (2010).
- ²⁰ O. Mosendz, J. E. Pearson, F. Y. Fradin, G. E. W. Bauer, S. D. Bader, and A. Hoffmann, *Phys. Rev. Lett.* **104**, 046601 (2010).
- ²¹ O. Mosendz, V. Vlaminck, J. E. Pearson, F. Y. Fradin, G. E. W. Bauer, S. D. Bader, and A. Hoffmann, *Phys. Rev. B* **82**, 214403 (2010).
- ²² P. Saraiva, A. Nogaret, J. C. Portal, H. E. Beere, and D. A. Ritchie, *Phys. Rev. B* **82**, 224417 (2010).
- ²³ Y. Kajiwara, K. Harii, S. Takahashi, J. Ohe, K. Uchida, M. Mizuguchi, H. Umezawa, H. Kawai, K. Ando, K. Takanashi, S. Maekawa, and E. Saitoh, *Nature(London)* **464**, 262 (2010).
- ²⁴ C. W. Sandweg, Y. Kajiwara, K. Ando, E. Saitoh, and B. Hillebrands, *Appl. Phys. Lett.* **97**, 252504 (2010).
- ²⁵ L. Liu, T. Moriyama, D. C. Ralph, and R. A. Buhrman *Phys. Rev. Lett.* **106**, 036601 (2011).
- ²⁶ A. Azevedo, L. H. Vilela-Leão, R. L. Rodríguez-Suárez, A. F. Lacerda Santos, and S. M. Rezende, *Phys. Rev. B* **83**, 144402 (2011).
- ²⁷ Y. S. Gui, N. Mecking, and C.-M. Hu, *Phys. Rev. Lett.* **98**, 217603 (2007).
- ²⁸ Y. S. Gui, A. Wirthmann, N. Mecking, and C.-M. Hu, *Phys. Rev. B* **80**, 060402(R) (2009).
- ²⁹ Y. S. Gui, A. Wirthmann, and C.-M. Hu, *Phys. Rev. B* **80**, 184422 (2009).
- ³⁰ C. T. Boone, J. A. Katine, J. R. Childress, V. Tiberkevich, A. Slavin, J. Zhu, X. Cheng, and I. N. Krivorotov, *Phys. Rev. Lett.* **103**, 167601 (2009).
- ³¹ D. Bedau, M. Kläui, S. Krzyk, U. Rüdiger, G. Faini and L. Vila, *Phys. Rev. Lett.* **99**, 146601 (2007).
- ³² S. Bonetti, V. Tiberkevich, G. Consolo, G. Finocchio, P. Muduli, F. Mancoff, A. Slavin, and J. Åkerman, *Phys. Rev. Lett.* **105**, 217204 (2010).
- ³³ S. Urazhdin, V. Tiberkevich, and A. Slavin, *Phys. Rev. Lett.* **105**, 237204 (2010).
- ³⁴ Y. Tserkovnyak, A. Brataas, G. E. W. Bauer, and B. I. Halperin, *Rev. Mod. Phys.* **77**, 1375 (2005).
- ³⁵ X. Wang, G. E. W. Bauer, B. J. van Wees, A. Brataas, and Y. Tserkovnyak, *Phys. Rev. Lett.* **97**, 216602 (2006).
- ³⁶ A. Yamaguchi, H. Miyajima, S. Kasai, and T. Ono, *Appl. Phys. Lett.* **90**, 212505 (2007).
- ³⁷ A. Wirthmann, X. Fan, Y. S. Gui, K. Martens, G. Williams, J. Dietrich, G. E. Bridges, and C.-M. Hu, *Phys. Rev. Lett.* **105**, 017202 (2010).
- ³⁸ X. F. Zhu, M. Harder, A. Wirthmann, B. Zhang, W. Lu, Y. S. Gui, and C.-M. Hu, *Phys. Rev. B* **83**, 104407 (2011).
- ³⁹ X. Fan, S. Kim, X. Kou, J. Kolodzey, H. Zhang, and J. Q. Xiao, *Appl. Phys. Lett.* **97**, 212501 (2010).
- ⁴⁰ L. H. Bai, Y. S. Gui, A. Wirthmann, E. Recksiedler, N. Mecking, C.-M. Hu, Z. H. Chen, and S. C. Shen, *Appl. Phys. Lett.* **92**, 032504 (2008).
- ⁴¹ H. Zhao, E. J. Loren, H. M. van Driel, and A. L. Smirl, *Phys. Rev. Lett.* **96**, 246601 (2006).
- ⁴² J. Wang, B. F. Zhu, and R. B. Liu, *Phys. Rev. Lett.* **104**, 256601 (2010).
- ⁴³ L. K. Werake, and H. Zhao, *Nature Physics*, **6**, 875 (2010).
- ⁴⁴ J. D. Jackson, *Classical Electrodynamics* (John Wiley & Sons, New York, 1975), 2nd ed.
- ⁴⁵ H. J. Juretschke, *J. Appl. Phys.* **31**, 1401 (1960).
- ⁴⁶ R. H. Silsbee, A. Janossy, and P. Monod, *Phys. Rev. B* **19**, 4382 (1979).
- ⁴⁷ B. Heinrich, Y. Tserkovnyak, G. Woltersdorf, A. Brataas, R. Urban, and G. E. W. Bauer, *Phys. Rev. Lett.* **90**, 187601 (2003).
- ⁴⁸ J. N. Kupferschmidt, S. Adam, and P. W. Brouwer, *Phys. Rev. B* **74**, 134416 (2006).
- ⁴⁹ A. A. Kovalev, G. E. W. Bauer, and A. Brataas, *Phys. Rev. B* **75**, 014430 (2007).
- ⁵⁰ T. L. Gilbert, *IEEE Trans. Magn.* **40**, 3443 (2004).
- ⁵¹ L. D. Landau and E. M. Lifshitz, *Mechanics*, second edition

- (Pergamon Press, Oxford, 1969).
- ⁵² J. P. Jan, in *Solid State Physics*, edited by F. Seitz and D. Turnbull (Academic, New York, 1957), Vol. 5.
- ⁵³ M. Born and E. Wolf, *Principles of optics: Electromagnetic theory of propagation, interference and diffraction*, 7th edition (Cambridge university press, Cambridge, 1999).
- ⁵⁴ W. Heinrich, IEEE Trans. Microwave Theory Tech. **38**, 1468 (1990).
- ⁵⁵ W. Heinrich, IEEE Trans. Microwave Theory Tech. **41**, 45 (1993).
- ⁵⁶ S. V. Vonsovskii, *Ferromagnetic Resonance: The Phenomenon of Resonant Absorption of a High-Frequency Magnetic Field in Ferromagnetic Substances*, (Oxford: Pergamon, 1966).
- ⁵⁷ B. S. Guru, and H. R. Hiziroğlu, *Electromagnetic Field Theory Fundamentals*, 2nd ed. (Cambridge University Press, Cambridge, England, 2004).
- ⁵⁸ V. Tiberkevich and A. Slavin, Phys. Rev. B **75**, 014440 (2007).